Methods for Multi-Loop Identification of Visual and Neuromuscular Pilot Responses

Mario Olivari, *Student Member, IEEE,* Frank M. Nieuwenhuizen, Joost Venrooij, *Student Member, IEEE,* Heinrich H. Bülthoff, *Member, IEEE,* and Lorenzo Pollini, *Member, IEEE*

Abstract

In this paper, identification methods are proposed to estimate the neuromuscular and visual responses of a multi-loop pilot model. A conventional and widely used technique for simultaneous identification of the neuromuscular and visual systems makes use of cross-spectral density estimates. This paper shows that this technique requires a specific *non-interference* hypothesis, often implicitly assumed, that may be difficult to meet during actual experimental designs. A mathematical justification of the necessity of the non-interference hypothesis is given. Furthermore, two methods are proposed that do not have the same limitations. The first method is based on ARX models, whereas the second one combines cross-spectral estimators with interpolation in the frequency domain. The two identification methods are validated by offline simulations and contrasted to the classic method. The results reveal that the classic method fails when the non-interference hypothesis is not fulfilled; on the contrary, the two proposed techniques give reliable estimates. Finally, the three identification methods are applied to experimental data from a closed-loop control task with pilots. The two proposed techniques give comparable estimates, different from those obtained by the classic method. The differences match those found with the simulations. Thus, the two identification methods provide a good alternative to the classic method and make it possible to simultaneously estimate a human's neuromuscular and visual response in cases where the classic method fails.

Index Terms

M. Olivari is with the Department of Human Perception, Cognition and Action, Max Planck Institute for Biological Cybernetics, 72076 Tübingen, Germany, and also with Dipartimento di Ingegneria dell'Informazione, University of Pisa, 56122 Pisa, Italy (e-mail: mario.olivari@tuebingen.mpg.de)

F. M. Nieuwenhuizen is with the Department of Human Perception, Cognition and Action, Max Planck Institute for Biological Cybernetics, 72076 Tübingen, Germany (e-mail: frank.nieuwenhuizen@tuebingen.mpg.de).

J. Venrooij is with the Department of Human Perception, Cognition and Action, Max Planck Institute for Biological Cybernetics, 72076 Tübingen, Germany, and also with the Faculty of Mechanical, Maritime and Materials Engineering, Delft University of Technology (TU Delft), 2628CD Delft, The Netherlands (e-mail: joost.venrooij@tuebingen.mpg.de).

L. Pollini is with Dipartimento di Ingegneria dell'Informazione, University of Pisa, 56122 Pisa, Italy (e-mail: lorenzo.pollini@unipi.it).

H. H. Bülthoff is with the Department of Human Perception, Cognition and Action, Max Planck Institute for Biological Cybernetics, 72076 Tübingen, Germany, and also with the Department of Brain and Cognitive Engineering, Korea University, Seoul 136-7601, Korea (e-mail: heinrich.buelthoff@tuebingen.mpg.de).

Pilot identification, neuromuscular system, haptic feedback, tracking task.

I. Introduction

Novel pilot support systems include haptic aids that help pilots perform a control task by providing additional tactile information on the control device [1]–[3]. Haptic aids have been widely employed in several contexts. Examples are remote control with the master-slave paradigm [1], [4], force feedback in servo-actuated systems [5], and robotic assisted surgery [6]. In these contexts the haptic channel is used to let the operator feel variations and/or discontinuities in the environment, like hitting or approaching an obstacle, encountering unexpected loads, or interacting with surfaces (i.e. tissues) with different softness. This knowledge eventually increases performance and situational awareness. Other studies investigated the use of haptic feedback for generating synthetic warnings. So-called stick shakers are currently used in many modern aircraft for alerting pilots to a potential stall [7], [8].

In recent years, there has been considerable interest in designing haptic aids as guidance systems. Such aids *continuously* provide a haptic feedback on the control device that suggests a possible right control action to the pilot. Examples are a haptic gas pedal that assists the driver in car following [9], a haptic steering wheel for lane-keeping [3], [10], and a haptic flight director that assists pilots in following a glide slope [11], [12]. The pilot can either follow the continuous haptic feedback, or override it in case of discordance. It has been shown that pilots quickly get acquainted with this type of haptic feedback, learn how to exploit it to increase their performance, and adapt their responses to the specific type of haptic aid [10], [13].

Due to the continuous nature of the tactile feedback, one can assume that pilots adopt a time-invariant behavior. Since humans can adapt their responses over a large range [13], [24], an effective design of haptic aid requires accurate knowledge of pilot adaptation to the provided continuous haptic feedback. This papers seeks to address how to model and estimate the pilot responses in control tasks with continuous haptic feedback.

Quasi-linear models are commonly used to describe pilot behavior in various control tasks [14]–[16]. These models represent pilot behavior with linear describing functions combined with a remnant signal to account for non-linearities. When haptic aids are used and tactile information is provided in addition to presenting visual information, the tactile perception channel needs to be modeled as an additional input to the pilot. A multi-loop quasi-linear model that meets this requirement was developed by van Paassen et al. [19], [20]. This model is characterized by two control loops, one describing the visual perception channel and one describing the tactile information processed by the neuromuscular system. Identifying the neuromuscular and visual responses would provide quantitative insights into the pilot adaptation to the haptic feedback.

To identify pilot visual and neuromuscular responses during a closed-loop control task, identification techniques are needed that account for the multi-loop nature of the task. A commonly used technique is based on the Cross Spectral Density (CSD) analysis [21]. This technique has been initially applied to neuromuscular system estimation for tasks in which pilot visual feedback is not involved and the pilot is essentially a single-input single-output system [22]. In [13], [23] the technique was extended to estimate neuromuscular system in control tasks with visual feedback. Two mutually uncorrelated forcing functions, a visual reference trajectory and a force

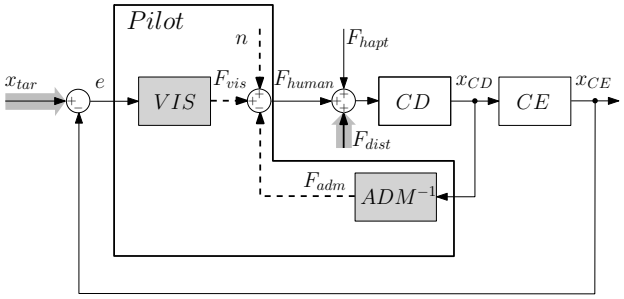

Fig. 1. Compensatory tracking task, in which a pilot controls the Controlled Element (CE) through a Control Device (CD). The pilot is described with a visual (VIS) and a neuromuscular response (the inverse of the admittance ADM), combined with the remnant signal n. The dashed arrows indicate signals that can not be measured, while the large shaded arrows represent the known forcing functions needed for identification. All other signals can be measured.

disturbance, were inserted in the feedback loop to estimate the neuromuscular and visual dynamics. The contribution of force disturbance in the visual error was implicitly assumed to be negligible, i.e., the force disturbance used for identification was assumed not to interfere with the visual feedback. Unfortunately, this *non-interference* assumption is not always verified [24]. As a sufficiently high Signal-to-Noise Ratio (SNR) is required for the identification procedure, the power of the force disturbance cannot be decreased such that its effect on the visual feedback is not actually perceived by the pilot.

This paper shows that the commonly used CSD method may provide biased estimates when the non-interference assumption is not fulfilled. Two novel identification methods are presented, which also produce reliable estimates when the force disturbance influences the visual error. In the first method (*ARX-method*), a multi-loop Auto-Regressive model with eXogenous inputs (ARX) is used to fit the measured data in the time domain. A similar identification procedure was successfully applied for a different control task [25]. The second method (*CSD-ML method*) makes use of the Cross Spectral Density analysis like the conventional method, but does not require the non-interference assumption. Numerical simulations and human in-the-loop experiment are performed to provide supportive evidence of the reliability of the two novel methods.

The paper is structured as follows: Section II presents a model that describes pilots in a tracking task with continuous haptic aids. Sections III and IV illustrate the theoretical basis of the three adopted identification methods, followed by a set of off-line Monte Carlo simulations in section V. Subsequently, section VI shows an experimental validation of the proposed identification methods. Finally, conclusions are drawn.

II. Pilot Model and Control Task Description

This paper focuses on human control behavior in a compensatory tracking task. In this task, pilots are asked to follow a reference signal by compensating for a tracking error e. When haptic aids are used, additional tactile information is provided to the pilot for achieving the control task. To assess the influence of this second input on the pilot, the visual and tactile perception channels need to be modeled separately.

A multi-loop model that meets these requirements was developed by van Paassen et al. [13], [19], see Fig. 1. The human operator is described by two control loops, the outer describing the visual response, whereas the inner loop describes the neuromuscular response. The neuromuscular response is represented by the inverse of the arm admittance ADM, defined as the dynamic relationship between the force acting on the arm and the position of the arm [13]. The visual system VIS and the neuromuscular response ADM both contribute to the control force F_{human}. As common in the context of pilot dynamics identification with continuous haptic aids [9], [13], the visual and the neuromuscular responses are assumed to be produced by linear and time-invariant systems. Nonlinearities in the pilot response are accounted for by the remnant signal n [15].

The haptic force F_{hapt} represents any additional force feedback provided by the haptic aid. In the field of guidance haptic aids, the haptic system is generally designed as a standard compensator, which continuously provides forces that aim at achieving a certain control task [24], [27]. Referring to the compensatory tracking task shown in Fig. 1, the haptic compensator is commonly designed to regulate the tracking error e to zero. Throughout this paper, we will consider the dynamics of the haptic compensator equal to zero for the purposes of developing the pilot identification techniques. This simplification does not affect the generality of the developed identification methods, since they are easily extensible to the case of non-zero haptic aid dynamics.

III. Conventional Identification Technique

This section describes the identification technique, based on cross-spectral analysis, that is commonly used to estimate the pilot responses of the model shown in Fig. 1. To simultaneously estimate the admittance and the visual response, two deterministic forcing functions need to be inserted into the loop: the target position x_{tar}, which represents the reference trajectory that pilot has to track, and the force disturbance F_{dist}, which represents a continuous force disturbance that the pilot can feel on the control device.

The forcing functions have to be tuned with care, as the presence of human in the control loop poses constraints on their power content. The amount of power and the bandwidth should not be too high, to prevent changes in the human control strategy [21], [28], [29]. At the same time, they should not be too low in order to ensure an accurate estimate. In order to satisfy both conflicting constraints simultaneously, a trade-off has to be found.

A. Forcing Functions Design

The two forcing functions x_{tar} and F_{dist} were designed as multisine signals [30]:

$$x_{tar}(t) = \sum_{j=1}^{N_t} T_j \sin(2\pi f_{T_j} t + \psi_{T_j}) \tag{1}$$

$$F_{dist}(t) = \sum_{j=1}^{N_d} D_j \sin(2\pi f_{D_j} t + \psi_{D_j}) \ . \tag{2}$$

Each frequency f_{D_j} and f_{T_j} was chosen as an integer multiple of the base frequency, which is defined as the inverse of the measurement time T of the forcing function. In this case, all measurements lasted 81.92 s, corresponding to a base frequency of 0.0122 Hz.

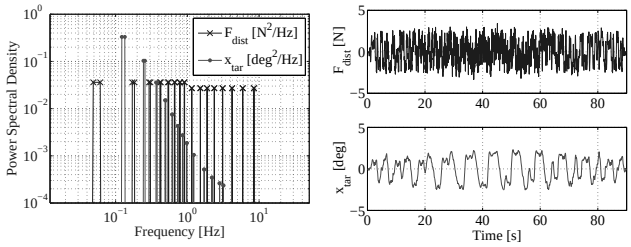

(a) Power Spectral Densities. (b) Sample realizations.

Fig. 2. Forcing signals x_{tar} and F_{dist}.

Simultaneously applying two forcing functions requires a method that allows distinguishing their contribution in the measurements. A well-documented method consists of assigning different sets of discrete points in the available frequency range to F_{dist} and x_{tar} [31], [32]. Fig. 2a shows the frequency separation of the two forcing signals used in this research. Each set of frequency points is composed of a cluster of two adjacent frequencies to allow for frequency averaging during estimation.

For both forcing functions, the phases ψ_i were chosen randomly to obtain unpredictable behavior. A cresting technique was applied to avoid peaks in the time domain [30], [33]. This technique minimizes the Cresting Factor (CF), which is defined as the maximum amplitude of the signal divided by the Root Mean Square (RMS) of the signal. By minimizing the cresting factor, the power of the signal can be higher without increasing the signal amplitude. The increased signal power generally results in better Signal-to-Noise Ratios (SNR), and, consequently, in better estimates.

The choice of signal amplitudes must account for human limitations. For the target position x_{tar}, the sinusoidal amplitudes at high frequencies should not be too large, since the pilot must be able to follow them. The amplitude distribution was chosen to match the frequency response of a filter H_f [25]:

$$H_f = \frac{(s+10)^2}{(s+1.25)^2} \ . \tag{3}$$

The amplitudes for F_{dist} were tuned to reach a trade-off between two conflicting objectives: they have to be low enough not to disturb pilots during the tracking task, but still allow distinguishing their contribution in the measurements. Furthermore, the "Reduced Power Method" was used [29], see Fig. 2a. The principle of this method is to apply a reduced power level at higher frequencies, to allow estimation in a wide range of frequencies without influencing the control behavior of pilots.

The multisine time signals were obtained from their spectra using the inverse Fast Fourier Transform [30]. Table I lists the base-frequency multiple k, the actual frequency f, the amplitude A and the phase ϕ of each of the sines in the forcing functions, and Fig. 2b shows a sample realizations of F_{dist} and x_{tar}.

B. Cross-Spectral Density Analysis

A common method for identification of control behavior is based on cross-spectral density estimates. This approach, referred to as the *CSD-based method*, has previously been used for pilots in a pitch tracking task [23], [26] and for car drivers in a car following task [31].

In a closed multi-loop system like in Fig. 1, the best linear approximation of the pilot admittance can be calculated as [21], [33]:

$$\hat{H}_{ADM}(f) = \frac{\hat{S}_{F_{dist}x_{CD}}(f)}{\hat{S}_{F_{dist}F_{adm}}(f)}, \qquad f \in \{f_d\} \tag{4}$$

where $\{f_d\}$ is the set of frequencies in which F_{dist} has power, $\hat{S}_{F_{dist}x_{CD}}$ and $\hat{S}_{F_{dist}F_{adm}}$ are the estimated cross-spectral densities between F_{dist} and x_{CD} and between F_{dist} and F_{adm}, respectively.

The CSD-based method assumes linearity of the pilot admittance; the validity of this assumption can be checked with the squared coherence function defined as [21]:

$$\hat{\Gamma}^2(f) = \frac{|\hat{S}_{F_{dist}x_{CD}}(f)|^2}{\hat{S}_{F_{dist}F_{dist}}(f)\hat{S}_{x_{CD}x_{CD}}(f)}, \qquad f \in \{f_d\}\ . \tag{5}$$

The coherence function $\hat{\Gamma}$ equals 1.0 when the system is linear and there is no noise, and approaches 0.0 when no linear relation is found.

To estimate the cross-spectral density $\hat{S}_{F_{dist}F_{adm}}$ in (4), the time realization of the force F_{adm} must be known. Unfortunately, only the total human force F_{human} on the control device can be measured, which is given by the sum of F_{adm} and F_{vis} (and the remnant noise n). However, if it is assumed that the visual response F_{vis} does not contain power at frequencies in $\{f_d\}$, the force F_{adm} at frequencies $\{f_d\}$ can be approximated with the human force F_{human} measured at frequencies $\{f_d\}$. In this case, the admittance at frequencies $\{f_d\}$ can be estimated given measurements of x_{CD}, F_{dist} and F_{human} as:

$$\hat{H}_{ADM}(f) = \frac{\hat{S}_{F_{dist}x_{CD}}(f)}{\hat{S}_{F_{dist}F_{adm}}(f)} \approx \frac{\hat{S}_{F_{dist}x_{CD}}(f)}{\hat{S}_{F_{dist}F_{human}}(f)},\ f \in \{f_d\}\ . \tag{6}$$

Note that only if the power of the tracking error e is zero for all frequencies $\{f_d\}$ does F_{vis} not contain power at frequencies in $\{f_d\}$. This is because the visual response VIS in Fig. 1 is considered linear. Therefore, to apply the common identification method, it must be assumed that the power of the tracking error e must be zero for all frequencies $\{f_d\}$: the *non-interference* assumption.

When the non-interference assumption is not fulfilled and F_{adm} cannot be approximated with F_{human}, the estimator in (6) actually estimates a transfer function different from the admittance. The estimated Frequency Response Function (FRF) can be written as:

$$\hat{H}_{ADM}(f) = \frac{\hat{S}_{F_{dist}x_{CD}}(f)}{\hat{S}_{F_{dist}F_{human}}(f)} = \frac{\hat{S}_{F_{dist}x_{CD}}(f) \Big/ \hat{S}_{F_{dist}F_{dist}}(f)}{\hat{S}_{F_{dist}F_{human}}(f) \Big/ \hat{S}_{F_{dist}F_{dist}}(f)} = \frac{\hat{H}_{F_{dist}x_{CD}}(f)}{\hat{H}_{F_{dist}F_{human}}(f)}, \qquad f \in \{f_d\} \tag{7}$$

where $\hat{H}_{F_{dist}x_{CD}}$ is the FRF from F_{dist} to x_{CD}, and $\hat{H}_{F_{dist}F_{human}}$ is the FRF from F_{dist} to F_{human}. Note that the transfer function $\hat{H}_{F_{dist}x_{CD}}$ is generally referred to as the *force disturbance feedthrough* [35]. Rearranging the

pilot model in Fig. 1, an analytical expression of $H_{F_{dist}F_{human}}$ is obtained as a function of the transfer functions H_{ADM}, H_{VIS}, H_{CE}, and H_{CD}, i.e.:

$$H_{F_{dist}F_{human}} = \frac{-H_{CD}(H_{CE}H_{VIS} + H_{ADM}^{-1})}{1 + H_{CD}(H_{CE}H_{VIS} + H_{ADM}^{-1})} = -\frac{H_{CD}H_{CE}H_{VIS}H_{ADM} + H_{CD}}{H_{ADM} + H_{CD}H_{CE}H_{VIS}H_{ADM} + H_{CD}} \ . \tag{8}$$

Similar steps are applied to find an analytical expression for the transfer function $H_{F_{dist}x_{CD}}$:

$$H_{F_{dist}x_{CD}} = \frac{\frac{H_{CD}H_{ADM}}{H_{ADM}+H_{CD}}}{1 + \frac{H_{CD}H_{ADM}}{H_{ADM}+H_{CD}}H_{VIS}H_{CE}} = \frac{H_{CD}H_{ADM}}{H_{ADM} + H_{CD} + H_{CD}H_{ADM}H_{VIS}H_{CE}} \ . \tag{9}$$

More details on obtaining the previous expressions is given in the Appendix. Dividing (9) by (8), an analytical expression of the estimated admittance is found:

$$\hat{H}_{ADM} = \frac{H_{F_{dist}x_{CD}}}{H_{F_{dist}F_{human}}} = \frac{H_{CD}H_{ADM}}{H_{CD}H_{CE}H_{VIS}H_{ADM} + H_{CD}} = \frac{H_{ADM}}{1 + H_{CE}H_{VIS}H_{ADM}} \ . \tag{10}$$

It is clear that (6) represents a biased estimate of the admittance. Only at those frequencies where the product of H_{VIS}, H_{CE}, and H_{ADM} is small compared to 1 ($H_{CE}H_{VIS}H_{ADM} \ll 1$), $\hat{H}_{ADM}$ approaches the real admittance H_{ADM}. Therefore, if the non-interference assumption is violated, the estimated admittance may become unreliable.

Another drawback of the CSD-based method is that the pilot visual response H_{VIS} can not be obtained directly, because the force F_{vis} can not be measured. On the contrary, the transfer function between the visual error e and the position of the controlled element x_{CE}, i.e., the open-loop transfer function, can be estimated using cross-spectra estimates [21], [33]. In this case, the target forcing function x_{tar} is considered as the external deterministic input uncorrelated with the remnant noise. The pilot open-loop FRF can be estimated as:

$$\hat{H}_{OL}(f) = \frac{\hat{S}_{x_{tar}x_{CE}}(f)}{\hat{S}_{x_{tar}e}(f)}, \qquad f \in \{f_t\} \tag{11}$$

where $\{f_t\}$ is the set of frequencies in which x_{tar} has power.

The coherence function corresponding to the open-loop transfer function is given by:

$$\hat{\Gamma}^2_{OL}(f) = \frac{|\hat{S}_{x_{tar}x_{CE}}(f)|^2}{\hat{S}_{x_{tar}x_{tar}}(f)\hat{S}_{x_{CE}x_{CE}}(f)}, \qquad f \in \{f_t\} \ . \tag{12}$$

IV. Novel Identification Techniques

To address the limitations of the conventional identification method described in the previous section, two novel identification techniques are presented. The first method operates in the time-domain and uses an AutoRegressive model with eXogenous inputs (ARX) to fit measured data. The second identification method operates in the frequency domain and uses cross-spectral density estimates similarly to the conventional technique. However, it does not require the non-interference assumption.

A. AutoRegressive models with eXogenous inputs

Linear Time-Invariant (LTI) polynomial models, such as the ARX, ARMAX, and Box-Jenkins (BJ) models, are commonly used for the identification of a large variety of dynamic systems [34]. These models describe the relationship between the system inputs, the noise and the system outputs with parametric rational transfer functions.

Based on time measurements of input and output signals of a generic dynamic system, an optimization procedure is used to find the LTI polynomial model that fits the time signals best.

Polynomial models were previously used to estimate human admittance during a car following task [31]. The driver model consisted of neuromuscular and visual responses as shown in Fig. 1. To identify the neuromuscular response, the response to the visual error e was treated as an external filtered Gaussian noise. Single-input BJ models were then used to estimate the neuromuscular response. Although this approach provided reliable neuromuscular estimate [31], it may fail when the response to the visual error e cannot be approximated as an external Gaussian noise.

The ARX method described in our paper explicitly accounts for the response to the visual error e by using a multi-input ARX method. The stick deflection x_{CD} can be considered as the output of a linear system that has a visual error e and a disturbance force F_{dist} as inputs, and that is perturbed by the remnant noise n (Fig. 1). A multi-input ARX model is then used to describe this dynamic system [34]:

$$\begin{aligned} x_{CD}(t) = H_e(q)e(t) + H_f(q)F_{dist}(t) + H_n(q)n(t) = \\ \frac{B_e(q)}{A(q)}e(t) + \frac{B_f(q)}{A(q)}F_{dist}(t) + \frac{1}{A(q)}N(t) \ , \end{aligned} \tag{13}$$

with:

$$A(q) = 1 + a_1 q^{-1} + \ldots + a_{n_a} q^{-n_a} \tag{14}$$

$$B_{e,f}(q) = b_{0_{e,f}} + b_{1_{e,f}} q^{-1} + \ldots + b_{n_{be,bf}} q^{-n_{n_{be,bf}}} \ . \tag{15}$$

H_e and H_f represent the transfer functions from e and F_{dist} to x_{CD}, respectively, which are related to the visual response H_{VIS} and the admittance H_{ADM}. The transfer function H_n models the effect of the remnant noise n on stick deflection. In the ARX model, this effect is represented by the white noise signal $N(t)$ filtered by the transfer function $\frac{1}{A(q)}$. The terms n_a, n_{be}, and n_{bf} are the order of the corresponding polynomials. It should be noted that all the transfer functions of the system have the same set of poles. Although this coupling may be unrealistic, simulations and experimental results in sections V and VI will show that this does not to affect the identification accuracy.

Given the measurements of x_{CD}, F_{dist}, and e, the polynomial orders and the parameter values of the ARX model are estimated as the optimal solution of a suitable cost function. In this paper, the Akaike final prediction error was used as the cost function [34]. The optimal least-squares solution comes in closed form as a linear regression, and does not suffer from local minima. It should be noted that this is not the case for other polynomial model structures like ARMAX and BJ [34].

No requirements need to be imposed on frequency separation between the inputs signals e and F_{dist} in order to obtain reliable estimates [25]. Thus, contrary to the CSD-based method, the ARX method does not require any assumption about possible interference of the feedback from F_{dist} with the visual error e.

The arm admittance, visual response and open loop transfer functions are obtained from H_e, H_f using block

diagram algebra:

$$\hat{H}_{ADM} = \frac{H_{CD} H_f}{H_{CD} - H_f} \tag{16}$$

$$\hat{H}_{VIS} = \frac{H_e}{H_f} \tag{17}$$

$$\hat{H}_{OL} = H_e H_{CE} \ . \tag{18}$$

An overall validity of the ARX models is assessed by the Variance Accounted For (VAF), which shows how well the model can predict the measured output signal [25]. The VAF is defined as:

$$VAF = \left[1 - \frac{\sum_{k=1}^{N} |x_{CD}(t_k) - \hat{x}_{CD,ARX}(t_k)|^2}{\sum_{k=1}^{N} |x_{CD}(t_k)|^2} \right] \times 100\% \tag{19}$$

where $x_{CD}(t_k)$ and $\hat{x}_{CD,ARX}(t_k)$ represent the measured and the predicted stick deflection, respectively (k indexes the time samples). The value of the VAF varies between 0% and 100%, where 100% indicates that the ARX model completely describes the measured system response. Lower values are an indication of a worse model fit due to noise, nonlinearities, or unmodeled system characteristics.

B. Multi-loop cross-spectral densities

This section presents a second novel identification method based on cross-spectral density estimates, which explicitly accounts for the multi-loop nature of the considered control task. This method, referred to as the CSD-ML method, does not require the non-interference hypothesis on the power content of the visual error e and does not assume a rigid predefined model structure as the ARX approach.

In the CSD-ML method, the cross-spectral density analysis is used to estimate the following auxiliary FRFs:

- the FRF of the transfer function $H_{x_{tar}x_{CD}}$ from the target position x_{tar} to the CD deflection x_{CD}, i.e.:

$$\hat{H}_{x_{tar}x_{CD}}(f) = \frac{\hat{S}_{x_{tar}x_{CD}}(f)}{\hat{S}_{x_{tar}x_{tar}}(f)}, \qquad f \in \{f_t\} \ . \tag{20}$$

- the FRF of the transfer function $H_{F_{dist}x_{CD}}$ from the force disturbance F_{dist} to the CD deflection x_{CD}, i.e., the so-called force disturbance feedthrough [35]:

$$\hat{H}_{F_{dist}x_{CD}}(f) = \frac{\hat{S}_{F_{dist}x_{CD}}(f)}{\hat{S}_{F_{dist}F_{dist}}(f)}, \qquad f \in \{f_d\} \ . \tag{21}$$

$\hat{H}_{x_{tar}x_{CD}}$ and $\hat{H}_{F_{dist}x_{CD}}$ represent closed-loop dynamics from x_{tar} and F_{dist} to x_{CD}, respectively. Therefore they include dynamics of admittance H_{ADM}, visual response H_{VIS}, controlled element H_{CE}, and control device H_{CD}, see Fig. 2. The feedback loop from F_{dist} to the visual error e is explicitly accounted for in the closed-loop dynamics. Thus, the presence of any frequency content originating from F_{dist} in the visual error does not represent a problem, as its effect on pilot behavior is explicitly accounted for.

The admittance $\hat{H}_{ADM}$ and visual response $\hat{H}_{VIS}$ are computed from $\hat{H}_{x_{tar}x_{CD}}$ and $\hat{H}_{F_{dist}x_{CD}}$ using block diagram algebra. This procedure requires that $\hat{H}_{x_{tar}x_{CD}}$ and $\hat{H}_{F_{dist}x_{CD}}$ must be known for a common set of

frequencies $\{\bar{f}\}$ over which they can be combined. Unfortunately, $\hat{H}_{x_{tar}x_{CD}}$ and $\hat{H}_{F_{dist}x_{CD}}$ are known only for the sets $\{f_t\}$ and $\{f_d\}$ respectively, which do not have frequency points in common. However, since it is reasonable to assume a "smooth" behavior of the frequency response functions $\hat{H}_{x_{tar}x_{CD}}$ and $\hat{H}_{F_{dist}x_{CD}}$, a linear interpolation between neighboring frequencies can be applied to obtain $\hat{H}_{x_{tar}x_{CD}}$ and $\hat{H}_{F_{dist}x_{CD}}$ on frequencies at which they are not known. The CSD-ML method uses interpolation to estimate $\hat{H}_{x_{tar}x_{CD}}$ in the set $\{f_d\}$ and $\hat{H}_{F_{dist}x_{CD}}$ in the set $\{f_t\}$. A similar interpolation approach was used in [35].

It should be noted that $\hat{H}_{x_{tar}x_{CD}}$ can only be interpolated on a limited subset of $\{f_d\}$, due to the design of disturbance forcing functions. As shown in Fig. 2, the frequency range of $\{f_d\}$ (0.05 Hz - 10 Hz) is larger than the frequency range of $\{f_t\}$ (0.1 Hz - 3 Hz). Since an interpolation of $\hat{H}_{x_{tar}x_{CD}}$ outside the range of $\{f_t\}$ would produce unreliable estimates, the interpolation procedure can only be applied to the frequencies of $\{f_d\}$ in the range 0.1 Hz - 3 Hz. The resulting set $\{\bar{f}\}$, in which both $\hat{H}_{x_{tar}x_{CD}}$ and $\hat{H}_{F_{dist}x_{CD}}$ could be estimated, contained all frequencies in $\{f_d\}$ and $\{f_t\}$ in the range 0.1 Hz - 3 Hz.

Analytical expressions for $H_{F_{dist}x_{CD}}$ and $H_{x_{tar}x_{CD}}$ can be given as functions of the various system transfer functions, see equations (9) and (22):

$$H_{x_{tar}x_{CD}} = \frac{H_{VIS}\frac{H_{CD}H_{ADM}}{H_{ADM}+H_{CD}}}{1+\frac{H_{CD}H_{ADM}}{H_{ADM}+H_{CD}}H_{VIS}H_{CE}} \ . \tag{22}$$

The derivation of these expressions is detailed in the Appendix. The FRFs of pilot admittance and visual response are estimated from (9) and (22) by using the estimated $\hat{H}_{x_{tar}x_{CD}}$ and $\hat{H}_{F_{dist}x_{CD}}$:

$$\hat{H}_{VIS}(f) = \frac{\hat{H}_{x_{tar}x_{CD}}(f)}{\hat{H}_{F_{dist}x_{CD}}(f)} \tag{23}$$

$$\hat{H}_{ADM}(f) = \frac{\hat{H}_{F_{dist}x_{CD}}(f)H_{CD}(f)}{H_{CD}(f) - H_{CD}(f)\hat{H}_{x_{tar}x_{CD}}(f)H_{CE}(f) - \hat{H}_{F_{dist}x_{CD}}(f)} \ . \tag{24}$$

Each FRF is calculated at the set of frequency points $\{\bar{f}\}$ resulting from the interpolation. In addition, the open-loop FRF $\hat{H}_{OL}$ from the visual error e to the CE position x_{CE} is calculated as:

$$\hat{H}_{OL}(f) = H_{CE}(f)\frac{\hat{H}_{x_{tar}x_{CD}}(f)}{1-\hat{H}_{x_{tar}x_{CD}}(f)H_{CE}(f)}, \quad f \in \{\bar{f}\} \ . \tag{25}$$

V. Off-line simulations

This section presents a comparison of the three identification techniques introduced in sections III and IV. A Monte-Carlo simulation of the multi-loop pilot model with a fixed remnant power was used to validate the identification methods. In addition, the effect of the controlled element gain on the accuracy of admittance estimation was assessed. Finally, the identification methods were tested with increasing levels of the remnant power in order to analyze their robustness.

A. Simulations with reference parameter values

The model in Fig. 1 was simulated with 100 different realizations of the remnant noise n, obtained as a Gaussian white noise filtered by a third-order-low-pass filter H_n [36]:

$$H_n(s) = K_N\frac{12.7^3}{(s+12.7)(s^2+2\cdot 0.26\cdot 12.7s+12.7^2)} \ . \tag{26}$$

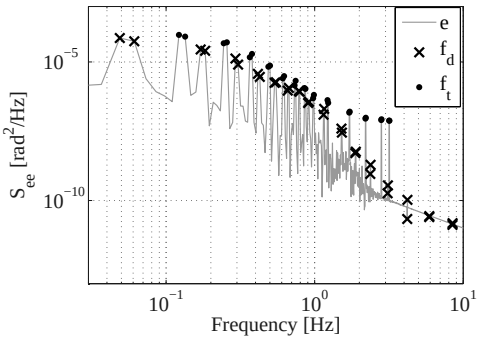

Fig. 3. A typical power spectral density plot of the simulated visual error e.

The value of the gain K_N was set to 2.12, in order to obtain a ratio of 0.5 between the remnant power and the power of the linear part of the pilot response: $F_{vis} - F_{adm}$.

All simulations used fixed dynamics for the dynamic elements in Fig. 1. The CE dynamics were modeled similar to a previous study [37]:

$$H_{CE}(s) = \frac{18}{s(s+3)} \qquad [rad/rad] \ . \tag{27}$$

The CD dynamics were based on the identified response of a control device from Wittenstein Aerospace & Simulation GmbH, Germany:

$$H_{CD}(s) = \frac{1}{1.522s^2 + 8.832s + 86.469} \qquad [rad/N] \ . \tag{28}$$

The parameters for the pilot model were derived from Damveld et al. [23] by adapting their values to match the measurements from experimental evaluations (section VI). Based on [23], the visual response was modeled by a gain, a lead-lag filter and a time delay:

$$H_{VIS}(s) = K_v \frac{1 + sT_{lead}}{1 + sT_{lag}} e^{-s\tau_v} \qquad [N/rad] \tag{29}$$

where $K_v = 20\,N/rad$, $T_{lead} = 0.3\,s$, $T_{lag} = 0.04s$, and $\tau_v = 0.2701\,s$. The model of the arm admittance was determined heuristically to fit the non-parametric estimation shown in [23]. The resulting transfer function is given by:

$$H_{ADM}(s) = \frac{4.566 \cdot 10^{-6}s^3 + 0.0046s^2 + 1.333s + 97.52}{s^3 + 82s^2 + 712.2s + 1.167 \cdot 10^{-4}} \qquad [rad/N] \ . \tag{30}$$

Fig. 3 shows a typical Power Spectral Density (PSD) of the simulated visual error e. The power of e is not negligible at frequencies $\{f_t\}$ and $\{f_d\}$ where x_{tar} and F_{dist} have power, respectively. This means that the force disturbance F_{dist} produces a large interference on the visual error e and the non-interference hypothesis is not fulfilled. Therefore, the CSD-based method is expected to provide biased estimates of neuromuscular response. In contrast, ARX and CSD-ML methods are expected to provide reliable estimates.

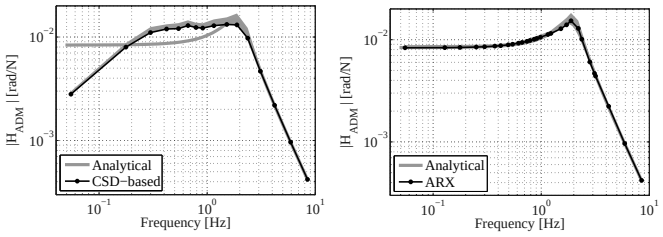

(a) CSD-based. (b) ARX.

(c) CSD-ML.

Fig. 4. Comparison between admittance estimates given by the three identification methods. The estimates are averaged over all the simulations, and the shaded areas show the (positive) standard deviation (mean + SD).

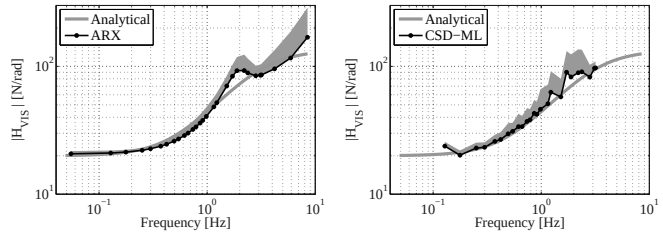

(a) ARX. (b) CSD-ML.

Fig. 5. Comparison between visual response estimates given by ARX and CSD-ML methods. The estimates are averaged over all the simulations, and the shaded areas show the (positive) standard deviation (mean + SD).

The admittance estimates given by the three identification methods are shown in Fig. 4. The CSD-based approach does not give correct estimates of the admittance at low frequencies, where the power level of e at the frequencies in $\{f_d\}$ is comparable to the power level at the frequencies in $\{f_t\}$ (see Fig. 3). On the contrary, both ARX and CSD-ML methods give good results. CSD-ML provides admittance estimate on a relatively small frequency range, due to interpolation.

The pilot visual response can only be directly estimated with the ARX and CSD-ML methods. Fig. 5 shows that both methods give reliable estimates. Finally, the estimated open-loop transfer function fits the simulated response well for all identification methods, see Fig. 6.

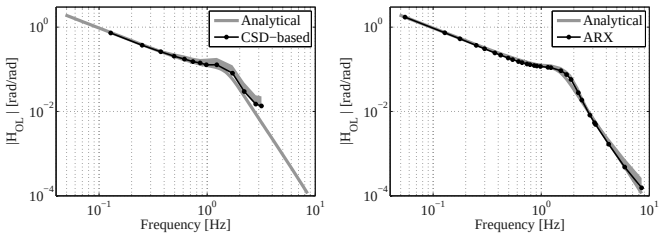

(a) CSD-based. (b) ARX.

(c) CSD-ML.

Fig. 6. Comparison between open-loop transfer function estimates given by the three identification methods. The estimates are averaged over all the simulations, and the shaded areas show the (positive) standard deviation (mean + SD).

B. Variation of the gain of the controlled element

As described in section III-B, admittance identified with the CSD-based method can be influenced to a large extent by the power content of the visual error e. High power content in the visual error signal e at frequencies $\{f_d\}$ results in a biased estimate. As shown in Eq. (10), the CSD-based method produces reliable estimates only at frequencies where $H_{CE}H_{VIS}H_{ADM} \ll 1$. This was investigated by performing multiple simulations with different values of the gain of the controlled element. It was hypothesized that the CSD-based method performs better with small gains of H_{CE}, whereas higher gains would result in a biased estimate of the admittance.

The dynamics for CD, ADM, VIS were the same as in section V-A. The CE dynamics was modeled as:

$$H_{CE} = K_{CE}\,\frac{3}{s(s+3)} \qquad [rad/rad]\ . \tag{31}$$

Five different values of K_{CE} were tested: 0, 3, 6, 9, 12. The condition $K_{CE} = 0$ represents an open-loop situation, where the non-interference hypothesis is completely fulfilled. No additional noise was inserted into the loop, as this effect will be tested explicitly in the next section.

Fig. 7 shows the admittance estimated by the three methods. As expected, the performance of the CSD-based method deteriorates with increasing values of K_{CE}. In contrast ARX and CSD-ML methods are not influenced by changes in the K_{CE} value.

It should be noted that, in a realistic scenario, pilots would adapt their behavior to the controlled element [38]. However, this section aimed to highlight the influence of non-interference hypothesis on the admittance estimation, and this effect becomes more clear when the pilot is considered invariant.

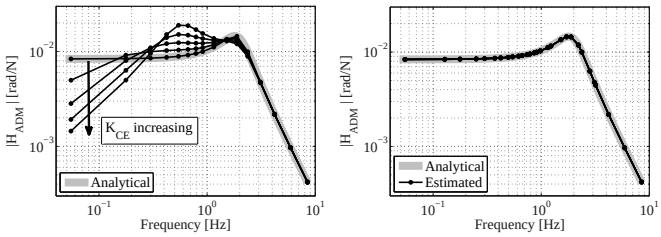

(a) CSD-based. (b) ARX.

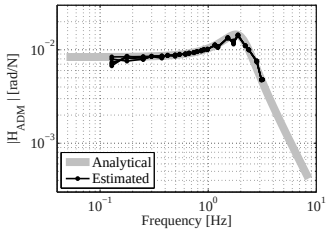

(c) CSD-ML

Fig. 7. Admittances estimated for different values of K_{CE} ($K_{CE} = 0, 3, 6, 9, 12$). The ARX and CSD-ML methods provide similar estimates for all values of K_{CE}.

C. Variation of the power of noise

The robustness of the three identification methods to increasing levels of pilot remnant was investigated by performing multiple simulations of the closed-loop control task with increasing levels of remnant noise power. The remnant gain K_N in (26) was gradually increased, resulting in 7 ratios between remnant power σ_N^2 and signal power σ_F^2, see table II. For each remnant level, 100 simulations were performed with different noise realizations. The analytical dynamics for CE, CD, ADM, VIS were chosen as in section V-A.

The admittance, the visual response and the open-loop transfer function were estimated by applying the three identification methods. To compare the performance of the methods, a cost function J was calculated, representing the logarithmic mean squared error between the estimated FRF ($\hat{H}$) and analytical FRF (H) [39]:

$$J = \frac{1}{N}\sum_{k=1}^{N}\left|\log\left(\frac{\hat{H}(f_k)}{H(f_k)}\right)\right|^2 . \tag{32}$$

This cost function accounts for both relative errors in the magnitude, and absolute errors in the phase. In order to obtain meaningful values, J was calculated considering the frequencies f_k that are common to the three identification methods, i.e., the frequencies in $\{f_d\}$ between 0.1 Hz and 3 Hz for admittance estimates, and the frequencies in $\{f_t\}$ for estimates of visual and open loop transfer functions.

Fig. 8 shows how cost function J varies with respect to the power ratio σ_N^2/σ_F^2. For all the estimates, J increases with increasing values of the remnant power, implying a growing discrepancy between analytical and estimated FRFs. The ARX method appears to be the most robust with respect to noise. This is due to the fact that the ARX method explicitly accounts for the remnant noise in the estimation procedure. Considering the admittance estimates,

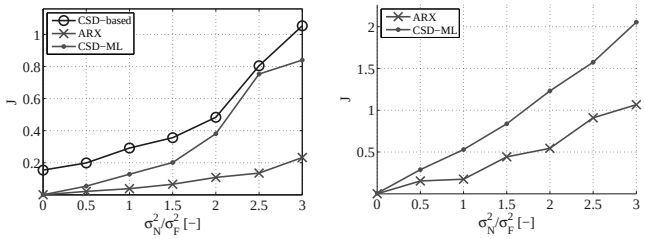

(a) Admittance.

(b) Visual response.

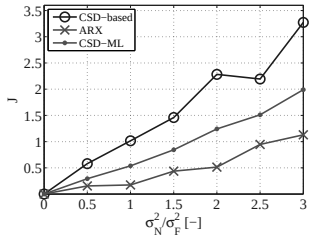

(c) Open loop transfer function.

Fig. 8. Averaged values of the cost function J for different remnant levels.

the CSD-based method also shows a non-zero value of J when the remnant noise has zero power, i.e., $\sigma_N^2/\sigma_F^2 = 0$ in Fig. 8a, indicating how the CSD-based method also provides a biased admittance estimate without remnant noise. Considering the visual response estimates, CSD-ML and ARX methods show a similar degradation of accuracy. Also for the open-loop transfer function estimates, the three methods show comparable degradation trends.

VI. Experimental evaluations

A. Method

The three identifications methods were applied to data obtained from an experimental manual control task. The experiment was performed using a control-loaded cyclic stick from Wittenstein Aerospace & Simulation GmbH, Germany, whose identified response dynamics are given in Eq. (28).

Eight participants performed a compensatory pitch tracking task and the roll axis of the stick was fixed. Before starting the experiment, participants received an overview about the scope of the experiment, and were instructed to minimize the tracking error shown on a primary flight display. The control device was continuously perturbed by a disturbance force. Both the reference signal and the disturbance force were designed as described in section III-A.

After a training phase, participants performed 8 experimental trials. Data were logged at 100 Hz and the last 2^{13} samples ($= 81.92$ s) of each trial of 90 s were used for identification purposes. Before identification, the data of the 8 trials performed by each participant were averaged in the time domain to reduce the effect of remnant noise. Fig. 9 illustrates the PSD of the error signal e, the human force F_{human}, the control signal x_{CD}, and the pitch angle x_{CE} for a single participant. The Signal-to-Noise Ratios (SNR) were high for most of the input frequencies of x_{tar} and F_{dist}.

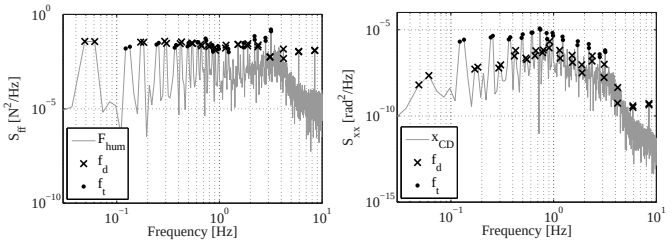

(a) Human force F_{human}. (b) Control device deflection x_{CD}.

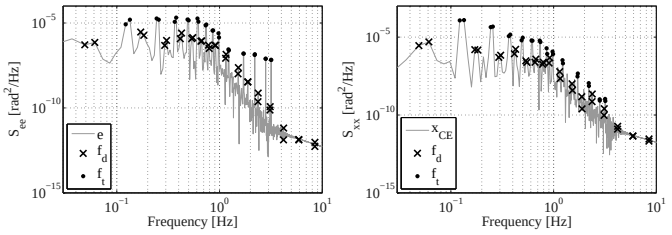

(c) Visual error e. (d) Pitch angle x_{CE}.

Fig. 9. Power spectral densities. The crosses and the points represent the disturbance force and target position frequencies, respectively.

The identification methods described in sections III and IV were then applied to the measured data. It was hypothesized that the CSD-based method would be influenced by the non-interference assumption, leading to estimates of admittance that differ from the ones obtained with the ARX and the CSD-ML methods. Furthermore, it was expected that the ARX and the CSD-ML provide similar admittance estimates.

B. Results

A sample PSD of the visual error is depicted in Fig. 9c. The power of e contained large peaks at frequencies $\{f_d\}$ where the force disturbance F_{dist} has power, especially at low frequencies. This indicates that F_{dist} had a large influence on the visual error e and the non-interference assumption of the CSD-based method was not fulfilled.

Fig. 10 shows the admittance identified by the three identification methods. The CSD-based method gives the admittance FRFs for all frequencies of $\{f_d\}$, while the CSD-ML method only provides admittance estimates below 3 Hz, which is the highest value in the frequency set $\{f_t\}$ as discussed in section IV-B. On the other hand, the ARX method provides a mathematical expression for the admittance transfer function, and the FRFs can be calculated for all the desired frequency points ($\{f_d\} \cup \{f_t\}$ in Fig. 10).

As expected, the admittance estimates given by ARX and CSD-ML were different from those given by the CSD-based technique, especially at lower frequencies. The admittance estimated by the CSD-method showed the same bias as found in simulations, see section V-A. At low frequencies ($f < 0.2$ Hz), the magnitude of the admittance estimated by CSD-based technique was lower than the magnitude given by the other two methods; the opposite occurred at medium frequencies (0.2 Hz $< f <$ 2 Hz); at higher frequencies the differences between methods disappeared. On the other hand, the ARX and CSD-ML methods provided similar estimates.

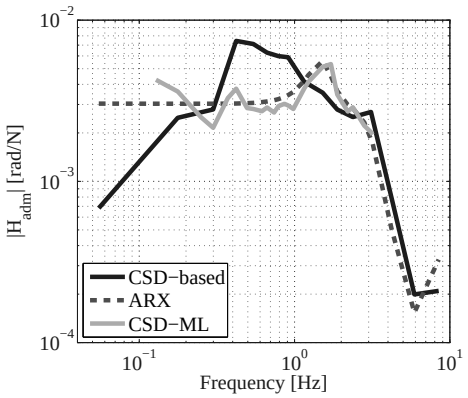

Fig. 10. Admittance frequency response functions for the three identification methods. The estimates are averaged over all participants.

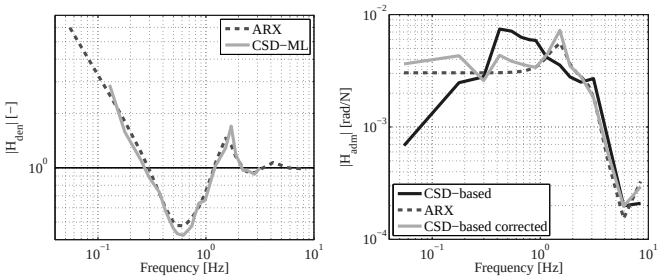

(a) (b)

Fig. 11. (a) Bias H_{den} of the admittance estimate by the CSD-based method. The bias is calculated using the FRFs estimated by the ARX and the CSD-ML methods. (b) Comparison between the admittance estimate by the CSD-based method and H_{ADM}/H_{den} estimate by the ARX and the CSD-ML methods. The dynamics H_{ADM}/H_{den} represent the biased admittance actually estimated by the CSD-based method.

Although the CSD-based method provided a biased admittance estimate, high squared coherence values were found at all frequencies ($\Gamma^2 > 0.8$). In fact, the coherence function does not give information about the correspondence between the actual and the estimated admittance, but only indicates that the relation between the measured human force F_{human} and the position of the control device x_{CD} can be approximated as linear. The estimates given by the ARX method were characterized by high VAF values (the mean value of the VAF was 87%), indicating that ARX models reproduce the measured signals well.

As shown in (10), the bias in the CSD-based method results from the admittance estimate including the dynamics of the visual response H_{VIS} and the controlled element H_{CE}. The bias is negligible only at those frequencies where $H_{den} = 1 - H_{VIS}H_{CE}H_{ADM}$ is close to 1, whereas it becomes larger when H_{den} diverges from 1. H_{den} can thus be used as a measure of the bias of the CSD-based estimate. To evaluate H_{den}, the actual dynamics of admittance H_{ADM} and visual responses H_{VIS} are required. Since these dynamics are not known a priori, the estimates provided by ARX and CSD-ML methods can be used. Fig. 11a shows that the resulting magnitude of H_{den} is close to 1 at

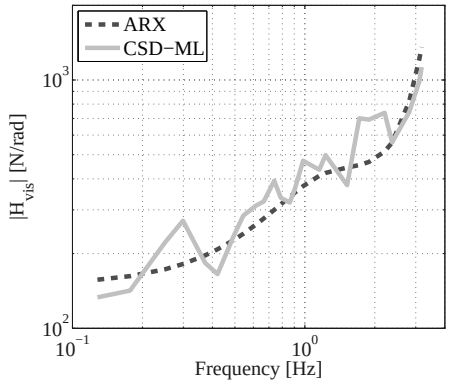

Fig. 12. Comparison between visual responses given by ARX and CSD-ML methods.

frequencies above 1 Hz, whereas it diverges from 1 at low frequencies. This is in complete agreement with results shown in Fig. 10.

The bias measure H_{den} can be used to correct the biased admittance given by the CSD-based method. The corrected admittance is obtained by multiplying the biased estimate by H_{den}, see (10). Fig. 11b shows the biased admittance given by CSD-based method, together with the corrected admittance and the ARX estimate. As the admittance estimate from the CSD-ML method was similar to the ARX estimate, it is not shown. As expected the corrected admittance is similar to the ARX estimate, confirming the validity of our analysis of the bias in the CSD-based method.

The pilot visual response can be computed directly only with ARX and CSD-ML methods. Fig. 12 shows that the estimates were comparable. The shape of the visual response resembled a gain at low frequencies and a differentiator at higher frequencies. The three identification methods gave comparable estimates also for the open-loop transfer function H_{OL} (Fig. 13). The open-loop responses resembled the dynamics of a single integrator at frequencies below 1 Hz. This correlates fairly well with McRuer's theories [14], which assess that pilots adapt their responses to yield integrator-like dynamics of the open-loop transfer function around the crossover frequency where $H_{OL} = 10^0$ rad/rad. The peak of the open-loop response at higher frequencies is related to the neuromuscular dynamics [14].

VII. Conclusions

Three techniques for simultaneous identification of pilot neuromuscular and visual responses have been investigated. We showed that the identification method commonly used in literature (CSD-based method) may give biased estimates of admittance in cases when a so-called *non-interference* assumption is not fulfilled. Furthermore, we have derived an analytic expression for the bias in the CSD-based admittance estimate.

We presented two different procedures, one based on ARX models and a multi-loop cross-spectral density method, which allow overcoming this limitation. The results of offline simulations confirmed that both the ARX and the

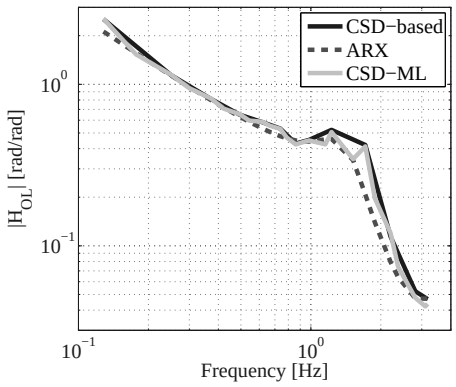

Fig. 13. Comparison between open-loop transfer function estimates given by the three identification methods.

CSD-ML methods give reliable estimates also in the case when the *non-interference* assumption is not satisfied.

The three identification methods were validated experimentally. The ARX and the CSD-ML methods showed estimates that were similar to each other, whereas the CSD-based method gave a biased estimate of admittance. Similar results were also found in simulation. The biased estimate of admittance from the CSD-based method could be corrected with experimental data, which corroborates our theoretical analysis of the CSD-based method.

Taken together, these results suggest that the admittance estimated by the CSD-based method cannot be considered to be reliable when the disturbance forcing function always has an influence on the visual error. On the contrary, the ARX and the CSD-ML methods are not influenced by the power content of the visual error.

The most important limitation of the ARX method lies in the fact that it assumes a rigid model structure that could be unrealistic. Despite this, the experimental results suggest that the ARX-model structure can describe our experimental data well. A number of potential limitations need to be considered also for the CSD-ML method. First, it gives admittance estimates in a reduced set of frequencies (at low frequencies with the forcing functions used in this paper). Furthermore, the interpolation procedure could yield noisy estimates. Nevertheless, we believe that this method could be a powerful tool to obtain an accurate low-frequency estimate when the influence of the disturbance force on the visual error is not negligible. The CSD-ML method neither makes a-priori hypothesis about the visual error, nor assumes a rigid model structure.

APPENDIX

In a closed-loop linear system as in Fig. 14a, the closed-loop transfer function H_{cl} between the input signal u and the output signal y is given by:

$$H_{cl} = \frac{H}{1 + H \cdot G} \tag{33}$$

where H and G represent the transfer functions of the system dynamics in the forward and feedback path, respectively.

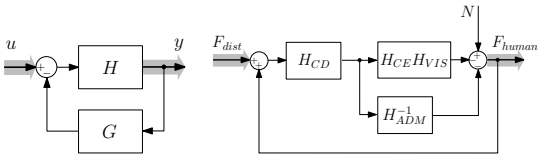

(a) Generic closed-loop system.

(b) Closed-loop system from F_{dist} to F_{human}.

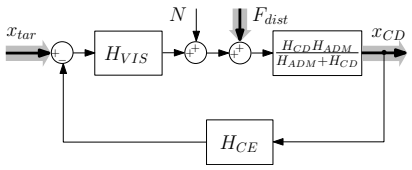

(c) Closed-loop systems from x_{tar} and F_{dist} to x_{CD}.

Fig. 14. Rearranged models of the compensatory tracking task in Fig. 1

The closed-loop dynamics between two generic signals of the compensatory tracking task in Fig. 1 can be obtained by rearranging the model to have a similar configuration as the system in Fig. 14a. Fig. 14b illustrates the rearranged model to obtain the dynamics between the disturbance force F_{dist} and the human force F_{human}. Here, the notation H_{SYS} indicates the transfer function of SYS. The forward and feedback transfer functions are given by:

$$H = H_{CD}(-H_{CE}H_{VIS} - H_{ADM}^{-1}), \qquad G = -1\,. \tag{34}$$

Fig. 14c shows the rearranged model to calculate the dynamics from x_{tar} and F_{dist} to x_{CD}. The forward and feedback transfer functions for the input signals x_{tar} and F_{dist} are:

$$x_{tar}: \quad H = H_{VIS}\frac{H_{CD}H_{ADM}}{H_{ADM}+H_{CD}}, \quad G = H_{CE} \tag{35}$$

$$F_{dist}: \quad H = \frac{H_{CD}H_{ADM}}{H_{ADM}+H_{CD}}, \quad G = H_{CE}H_{VIS} \tag{36}$$

ACKNOWLEDGMENTS

The work in this paper was partially supported by the myCopter project, funded by the European Commission under the 7th Framework Program. Heinrich H. Bülthoff was supported by the Brain Korea 21 PLUS Program through the National Research Foundation of Korea funded by the Ministry of Education. Correspondence should be directed to Heinrich H. Bülthoff.

REFERENCES

[1] T. M. Lam, M. Mulder, and M. M. van Paassen, "Haptic Interface in UAV Tele-Operation Using Force-Stiffness Feedback," in *Proc. IEEE Conf. Syst. Man Cybern.*, San Antonio, Texas, Oct. 2009, pp. 835 –840.

[2] S. Alaimo, L. Pollini, J.-P. Bresciani, and H. H. Bülthoff, "A Comparison of Direct and Indirect Haptic Aiding for Remotely Piloted Vehicles," in *Proc. 19th IEEE Ro-Man*, Viareggio, Italy, Sep. 2010, pp. 506–512.

[3] T. Brandt, T. Sattel, and M. Bohm, "Combining Haptic Human-Machine Interaction with Predictive Path Planning for Lane-Keeping and Collision Avoidance Systems," in *IEEE Intell. Veh. Symp.*, Eindhoven, The Netherlands, Jun. 2007, pp. 582–587.

[4] K. Hashtrudi-Zaad and S. E. Salcudean, "Transparency in Time-Delayed Systems and the Effect of Local Force Feedback for Transparent Teleoperation," *IEEE J. Robot. Autom.*, vol. 18, no. 1, pp. 108–114, 2002.

[5] N. Parker, S. Salcudean, and P. Lawrence, "Application of Force Feedback to Heavy Duty Hydraulic Machines," in *Proc. IEEE Int. Conf. Robot. Autom.*, vol. 1, Atlanta, GA, May 1993, pp. 375–381.

[6] J. Rosen, B. Hannaford, M. MacFarlane, and M. Sinanan, "Force Controlled and Teleoperated Endoscopic Grasper for Minimally Invasive Surgery - Experimental Performance Evaluation," *IEEE Trans. Biomed. Eng.*, vol. 46, no. 10, pp. 1212–1221, 1999.

[7] G. P. Boucek Jr, J. E. Veitengruber, and W. D. Smith, "Aircraft Alerting Systems Criteria Study. Volume II. Human Factors Guidelines for Aircraft Alerting Systems," Boeing Commercial Airplane Co., Seattle, WA, Tech. Rep. D6-44200, 1977.

[8] R. H. Cook, "An Automatic Stall Prevention Control for Supersonic Fighter Aircraft," *J. Aircraft*, vol. 2, no. 3, pp. 171–175, May/Jun. 1965.

[9] D. A. Abbink and M. Mulder, "Exploring the Dimensions of Haptic Feedback Support in Manual Control," *J. of Computing and Information Science in Engineering*, vol. 9, no. 1, pp. 011 006–1 – 011 006–9, Mar. 2009.

[10] L. Profumo, L. Pollini, and D. A. Abbink, "Direct and Indirect Haptic Aiding for Curve Negotiation," in *Proc. IEEE Conf. Syst. Man Cybern.*, Manchester, UK, Oct. 2013, pp. 1846–1852.

[11] K. Goodrich, P. Schutte, and R. Williams, "Haptic-Multimodal Flight Control System Update," in *Proc. 11th AIAA Aviation Technol., Integr., and Operations (ATIO) Conf.*, no. AIAA Paper 2011-6984, Virginia Beach, VA, Sep. 2011, pp. 1–17.

[12] S. De Stigter, M. Mulder, and M. M. Van Paassen, "Design and Evaluation of Haptic Flight Director." *J. Guidance Control Dyn.*, vol. 30, no. 1, pp. 35–46, Jan. 2007.

[13] D. A. Abbink, M. Mulder, F. C. T. van der Helm, M. Mulder, and E. R. Boer, "Measuring Neuromuscular Control Dynamics During Car Following with Continuous Haptic Feedback," *IEEE Trans. Syst., Man, Cybern. B*, vol. 41, no. 5, pp. 1239–1249, 2011.

[14] D. T. McRuer, "Human pilot dynamics in compensatory systems: Theory, models and experiments with controlled element and forcing function variations," Air Force Flight Dynamics Laboratory, Research and Technology Division, Air Force Systems Command, Wright-Patterson Air Force Base, OH, Tech. Rep. AFFDL-TR-65-15, 1965.

[15] D. T. McRuer and H. R. Jex, "A review of quasi-linear pilot models," *IEEE Trans. Hum. Factors Electron.*, vol. HFE-8, no. 3, pp. 231 – 249, Sep. 1967.

[16] R. A. Hess, "Pursuit Tracking and Higher Levels of Skill Development in the Human Pilot," *IEEE Trans. Syst., Man, Cybern.*, vol. 11, no. 4, pp. 262–273, Apr. 1981.

[17] D. T. McRuer, I. L. Ashkenas, and H. R. Pass, "Analysis of multiloop vehicular control systems," Defense Technical Information Center, Wright-Patterson Air Force Base, OH, Tech. Rep. ASD-TDR-62-1014, 1964.

[18] R. L. Stapleford, D. T. McRuer, and R. E. Magdaleno, "Pilot Describing Function Measurements in a Multiloop Task," *IEEE Transactions on Human Factors in Electronics*, vol. 8, no. 2, pp. 113–125, Jun. 1967.

[19] M. M. van Paassen, "Biophysics in Aircraft Control, A Model of the Neuromuscular System of the Pilot's Arm," Ph.D. dissertation, Delft Univ. of Technol., Delft, The Netherlands, 1994.

[20] M. M. van Paassen and M. Mulder, "Identification of Human Operator Control Behaviour in Multiple-Loop Tracking Tasks," in *Proc. 7th IFAC/IFIP/IFORS/IEA Symp. Anal. Design, Eval. Human-Mach. Syst.*, Kyoto, Japan, 1998, pp. 515–520.

[21] F. C. T. van der Helm, A. C. Schouten, E. de Vlugt, and G. G. Brouwn, "Identification of Intrinsic and Reflexive Components of Human Arm Dynamics during Postural Control," *J. Neurosci. Methods*, vol. 119, no. 1, pp. 1 – 14, May 2002.

[22] D. A. Abbink, "Task Instruction: The Largest Influence on Human Operator Motion Control Dynamics," in *Proc. Sec. Joint EuroHaptics Conf. and Symp. on Haptic Interfaces for Virt. Environment and Teleoperator Systems*, Tsukuba, Japan, Mar. 2007, pp. 206 –211.

[23] H. J. Damveld, D. A. Abbink, M. Mulder, M. Mulder, M. M. van Paassen, F. C. T. van der Helm, and R. J. A. W. Hosman, "Identification of the Feedback Component of the Neuromuscular System in a Pitch Control Task," in *Proc. AIAA Guidance Navigation Control Conf.*, no. AIAA 2010-7915, Toronto, Ontario Canada, Aug. 2010, pp. 1–22.

[24] M. Olivari, F. M. Nieuwenhuizen, J. Venrooij, H. H. Bülthoff, and L. Pollini, "Multi-loop Pilot Behaviour Identification in Response to Simultaneous Visual and Haptic Stimuli," in *Proc. AIAA Model. and Simul. Technol. Conf.*, no. AIAA 2012-4795, Minneapolis, Minnesota, Aug. 2012, pp. 1–23.

[25] F. M. Nieuwenhuizen, P. M. T. Zaal, M. Mulder, M. M. van Paassen, and J. A. Mulder, "Modeling Human Multichannel Perception and Control Using Linear Time-Invariant Models," *J. Guidance Control Dyn.*, vol. 31, no. 4, pp. 999–1013, Jul./Aug. 2008.

[26] H. J. Damveld, D. A. Abbink, M. Mulder, M. Mulder, M. M. van Paassen, F. C. T. van der Helm, and R. J. A. W. Hosman, "Measuring the Conribution of the Neuromuscular System During a Pitch Control Task," in *Proc. AIAA Model. and Simul. Technol. Conf.*, no. AIAA-2009-5824, Chicago, Illinois, Aug. 2009, pp. 1–19.

[27] D. A. Abbink, E. R. Boer, and M. Mulder, "Motivation for Continuous Haptic Gas Pedal Feedback to Support Car Following," in *IEEE Intell. Veh. Symp.*, Jun. 2008, pp. 283–290.

[28] A. C. Schouten, E. de Vlugt, B. J. van Hilten, and F. C. T. van der Helm, "Quantifying Proprioceptive Reflexes During Position Control of the Human Arm," *IEEE Trans. Biomed. Eng.*, vol. 55, no. 1, pp. 311 –321, Jan. 2008.

[29] W. Mugge, D. A. Abbink, and F. C. T. van der Helm, "Reduced Power Method: How to Evoke Low-Bandwidth Behaviour while Estimating Full-Bandwidth Dynamics," in *Proc. IEEE 10th Int. Conf. Rehabilitation Robot. ICORR*, Noordwijk, The Netherlands, Jun. 2007, pp. 575–581.

[30] A. C. Schouten, E. de Vlugt, and F. C. T. van der Helm, "Design of Perturbation Signals for the Estimation of Proprioceptive Reflexes." *IEEE Trans. Biomed. Eng.*, vol. 55, no. 5, pp. 1612–9, 2008.

[31] D. A. Abbink, "Neuromuscular Analysis of Haptic Gas Pedal Feedback during Car Following," Ph.D. dissertation, Delft Univ. of Technol., Delft, The Netherlands, Dec. 2006.

[32] J. Venrooij, D. A. Abbink, M. Mulder, and M. M. van Paassen, "A Method to Measure the Relationship Between Biodynamic Feedthrough and Neuromuscular Admittance," *IEEE Trans. Syst., Man, Cybern. B*, vol. 41, no. 4, pp. 1158 –1169, Aug. 2011.

[33] R. Pintelon and J. Schoukens, *System Identification: a Frequency Domain Approach*. Piscataway, NJ: IEEE Press, 2001.

[34] L. Ljung, *System Identification: Theory for the User*, 2nd ed. Englewood Cliffs, NJ: Prentice Hall, 1999.

[35] J. Venrooij, M. Mulder, D. A. Abbink, M. M. van Paassen, F. C. van der Helm, H. H. Bulthoff, and M. Mulder, "A New View on Biodynamic Feedthrough Analysis: Unifying the Effects on Forces and Positions," *IEEE Trans. Cybern.*, vol. 43, no. 1, pp. 129–142, Feb. 2013.

[36] P. M. T. Zaal, D. M. Pool, Q. P. Chu, M. M. van Paassen, M. Mulder, and J. A. Mulder, "Modeling Human Multimodal Perception and Control Using Genetic Maximum Likelihood Estimation," *J. Guidance Control Dyn.*, vol. 32, no. 4, pp. 1089–1099, 2009.

[37] R. A. Hess, "Modeling the Effects of Display Quality upon Human Pilot Dynamics and Perceived Vehicle Handling Qualities," *IEEE Trans. Syst., Man, Cybern.*, vol. 25, no. 2, pp. 338 –344, Feb. 1995.

[38] D. T. McRuer and D. H. Weir, "Theory of manual vehicular control," *Ergonomics*, vol. 12, no. 4, pp. 599–633, 1969.

[39] R. Pintelon, P. Guillaume, Y. Rolain, J. Schoukens, and H. Van Hamme, "Parametric Identification of Transfer Functions in the Frequency Domain - a Survey," *IEEE Trans. Autom. Control*, vol. 39, no. 11, pp. 2245 –2260, Nov. 1994.

[40] A. van Lunteren, "Identification of Human Operator Describing Function Models with One or Two Inputs in Closed Loop Systems," Ph.D. dissertation, Delft Univ. of Technol., Delft, The Netherlands, Jan. 1979.

Mario Olivari (S'14) received the M.Sc. degree in automation engineering *(cum laude)* from the University of Pisa, Pisa, Italy, in October 2012, for his work on the identification of pilot control behavior in a closed-loop control task with haptic aids. Currently, he is a Ph.D student in the context of a collaborative project between the Department of Human Perception, Cognition and Action at the Max Planck Institute for Biological Cybernetics, Tübingen, Germany, and the Faculty of Automation Engineering at the University of Pisa.

His research interests include haptic guidance systems, pilot identification and the modeling of the neuromuscular system.

Frank M. Nieuwenhuizen received his M.Sc. degree in aerospace engineering from Delft University of Technology in 2005 for work on the identification of pilot control behavior in a closed-loop control task and its experimental application. In 2012, he received his Ph.D. degree for his research into the influence of simulator motion system characteristics on pilot control behavior, a collaboration between the Department of Human Perception, Cognition and Action at the Max Planck Institute for Biological Cybernetics and the Faculty of Aerospace Engineering at Delft University of Technology.

He is currently project leader for the myCopter project, which is funded by the European Commission under the Seventh Framework Programme.

Joost Venrooij (S10) received his M.Sc. and Ph.D. degrees *(cum laude)* in Aerospace Engineering from Delft University of Technology, The Netherlands, in August 2009 and March 2014 respectively, for his work on biodynamic feedthrough. Since December 2010 he is working in a collaborative project between the Delft University of Technology and the Max Planck Institute for Biological Cybernetics.

His research interests include biodynamic feedthrough, haptics, and motion perception.

Heinrich H. Bülthoff (M'95) received his Ph.D. degree in natural sciences in 1980 from Eberhard Karls University, Tübingen, Germany.

From 1980 to 1985, he was Research Scientist with the Max Planck Institute (MPI) for Biological Cybernetics, Tübingen, and from 1985 to 1988 Visiting Scientist at the Massachusetts Institute of Technology, Cambridge. Between 1988 and 1993, he was Assistant Professor, Associate Professor and finally Full Professor of Cognitive Science at Brown University, Providence, RI. In 1993, he became the Director of the Department of Human Perception, Cognition and Action at the MPI for Biological Cybernetics, and scientific member of the Max Planck Society. Since 1996, he has been Honorary Professor with the Eberhard Karls University, and since 2009 Adjunct Professor with Korea University, Seoul, Korea.

His research interests include object recognition and categorization, perception and action in virtual environments, and human-robot interaction.

Lorenzo Pollini (M'93) received the "Laurea" degree in computer engineering *(cum laude)* and the Ph.D. degree in robotics and industrial automation from University of Pisa, Pisa, Italy, in 1997 and 2000, respectively.

From 2000 to 2002, he was an Instructor of Automatic Control with the Italian Navy Academy. He is currently an Assistant Professor of automatic control with the Faculty of Engineering, University of Pisa.

His research interests concern guidance and navigation systems, vision based control, haptic support systems, fuzzy and nonlinear adaptive control, and real time dynamic systems simulation with specific application to unmanned systems.

TABLE I

FREQUENCIES, AMPLITUDES, AND PHASES DEFINING THE DISTURBANCE AND TARGET FORCING FUNCTIONS.

Disturbance F_{dist}				Target x_{tar}			
k	f	A	ϕ	k	f	A	ϕ
(-)	(Hz)	(N)	(rad)	(-)	(Hz)	(N)	(rad)
4	0.0488	0.3810	1.3875	10	0.1221	0.0198	-0.7003
5	0.0610	0.3810	2.5511	11	0.1343	0.0198	2.2216
14	0.1709	0.3810	2.7917	20	0.2441	0.0111	4.5432
15	0.1831	0.3810	-0.4228	21	0.2563	0.0111	4.3424
24	0.2930	0.3810	-2.9281	30	0.3662	0.0065	4.5408
25	0.3052	0.3810	-1.8836	31	0.3784	0.0065	6.6869
34	0.4150	0.3810	-3.6960	40	0.4883	0.0042	4.6231
35	0.4272	0.3810	-4.1771	41	0.5005	0.0042	5.8999
44	0.5371	0.3810	-2.6694	50	0.6104	0.0030	8.3374
45	0.5493	0.3810	-3.5128	51	0.6226	0.0030	7.1502
54	0.6592	0.3810	-2.6805	60	0.7324	0.0023	7.4114
55	0.6714	0.3810	-0.1215	61	0.7446	0.0023	5.1712
64	0.7813	0.3810	2.9424	70	0.8545	0.0018	8.4636
65	0.7935	0.3810	2.8250	71	0.8667	0.0018	9.6620
74	0.9033	0.3810	-0.0129	80	0.9766	0.0015	8.6567
75	0.9155	0.3810	-1.2966	81	0.9888	0.0015	9.8456
94	1.1475	0.3302	2.2066	100	1.2207	0.0011	8.1844
95	1.1597	0.3302	2.0687	101	1.2329	0.0011	8.1368
124	1.5137	0.3302	0.1803	140	1.7090	0.0008	5.7817
125	1.5259	0.3302	0.4412	141	1.7212	0.0008	6.0687
154	1.8799	0.3302	3.8712	180	2.1973	0.0006	9.5528
155	1.8921	0.3302	3.7964	181	2.2095	0.0006	10.5519
194	2.3682	0.3302	0.4953	230	2.8076	0.0006	7.6383
195	2.3804	0.3302	1.6589	231	2.8198	0.0006	8.0429
254	3.1006	0.3302	2.1529	260	3.1738	0.0005	7.0004
255	3.1128	0.3302	-0.8407	261	3.1860	0.0005	6.3912
344	4.1992	0.3302	-0.2912				
345	4.2114	0.3302	2.0218				
484	5.9082	0.3302	4.7341				
485	5.9204	0.3302	8.1897				
694	8.4717	0.3302	5.8242				
695	8.4839	0.3302	9.2787				

TABLE II

SIMULATED POWER RATIOS.

K_N	0	2.21	3.5	4.6	6	7.6	10
σ_N^2/σ_F^2	0	0.5	1	1.5	2	2.5	3